Structure, Vol. 10, 837–849, June, 2002, ©2002 Elsevier Science Ltd. All rights reserved. PII S0969-2126(02)00774-8

Structure at 1.9 Å Resolution of a Quinohemoprotein Alcohol Dehydrogenase from *Pseudomonas putida* HK5

Zhi-wei Chen,[1] Kazunobu Matsushita,[2] Tetsuo Yamashita,[2] Taka-aki Fujii,[2] Hirohide Toyama,[2] Osao Adachi,[2] Henry D. Bellamy,[3,5] and F. Scott Mathews[1,4]

[1]Department of Biochemistry and Molecular Biophysics
Washington University School of Medicine
St. Louis, Missouri 63110

[2]Department of Biological Chemistry
Yamaguchi University
Yamaguchi 753-8515
Japan

[3]Stanford Synchrotron Radiation Laboratory
Stanford, California 94309

Summary

The type II quinohemoprotein alcohol dehydrogenase of *Pseudomonas putida* is a periplasmic enzyme that oxidizes substrate alcohols to the aldehyde and transfers electrons first to pyrroloquinoline quinone (PQQ) and then to an internal heme group. The 1.9 Å resolution crystal structure reveals that the enzyme contains a large N-terminal eight-stranded β propeller domain (~60 kDa) similar to methanol dehydrogenase and a small C-terminal c-type cytochrome domain (~10 kDa) similar to the cytochrome subunit of *p*-cresol methylhydoxylase. The PQQ is bound near the axis of the propeller domain about 14 Å from the heme. A molecule of acetone, the product of the oxidation of isopropanol present during crystallization, appears to be bound in the active site cavity.

Introduction

Many Gram-negative aerobic bacteria contain periplasmic enzymes that catalyze the oxidation of alcohols and sugars independent of pyridine nucleotides and contain noncovalently bound pyrroloquinoline quinone (PQQ) (Figure 1) as their redox cofactor [1]. These quinoproteins generally follow a ping-pong mechanism in which a pair of electrons is transferred from the substrate to the PQQ to produce the reduced cofactor intermediate (the reductive half reaction), after which the PQQ is reoxidized through delivery of the reducing equivalents one at a time along an electron transfer chain to a terminal oxidase in the cytoplasmic membrane (the oxidative half reaction). They are found in both soluble and membrane-associated forms. In the soluble enzymes, delivery of the electron to the membrane is generally mediated by small electron carrier proteins such as cytochromes and cupredoxins, whereas in the membrane-bound enzymes, the electrons are delivered to ubiquinone. The best-known example of a PQQ-containing enzyme is methanol dehydrogenase (MDH) isolated from methylotrophic bacteria [2].

In nonmethylotrophic bacteria, there are three classes of quinoprotein alcohol dehydrogenase (ADH) [3]. Type I ADH, isolated from pseudomonads, is a soluble, dimeric enzyme of identical subunits of ~60–65 kDa containing PQQ, but no other redox cofactors [4]. Type II ADH is a monomeric, soluble quinohemoprotein of ~70–75 kDa, and it is found in several different pseudomonads and related strains [5–9]. It contains PQQ and covalently bound heme. Type III ADH is a membrane-bound complex of three subunits that catalyzes the oxidation of ethanol and the subsequent reduction of ubiquinone within the cytoplasmic membrane [3]. The enzyme is found only in acetic acid bacteria. One of the subunits (~75 kDa) contains one PQQ and one heme c per monomer, another (~50 kDa) is a three-heme cytochrome, and the third (~14 kDa) has no cofactor.

Pseudomonas putida HK5 produces three different quinoprotein ADHs, one type I ADH and two type II ADHs [5]. When the bacteria are grown on ethanol, type I ADH is produced, whereas growth on butanol induces ADH IIB, and ADH IIG is induced by either 1,2-propanediol or glycerol. ADH IIB exhibits high activity against long-chain primary and secondary alcohols, while ADH IIG has a higher activity to diols but not to primary and secondary alcohols [5].

During the reductive half reaction, type I ADH and MDH show a similar, relatively narrow specificity for small substrates compared with type II ADHs, although MDH is able to oxidize methanol with 10^4-fold higher catalytic efficiency than type I ADH [10]. Type II ADHs are much more divergent with respect to substrate specificity, as shown for ADH IIB and ADH IIG, and have also been found to oxidize secondary alcohols, polyols, heterocyclic alcohols, polyethylene glycol, or polyvinyl alcohol, most of which are xenobiotic [7–9]. Thus, structural analysis of ADH IIB is important for understanding its broad substrate specificity.

Electron transfer during the oxidative half reaction differs among the three types of quinoprotein ADHs. Type I ADH, like MDH, has been shown to donate electrons directly to a soluble cytochrome c, while membrane-bound type III ADHs are known to donate electrons into the membranous ubiquinone pool [1]. In the type II ADHs, this process is believed to begin with an intramolecular electron transfer from PQQ to the covalently bound heme, although this reaction has not been thoroughly characterized as yet in the case of the quinohemoprotein ADH IIB. In vitro, potassium ferricyanide can serve as an artificial electron acceptor for ADH IIB, as well as for type III ADH, but not for MDH or type I ADH. An azurin, also isolated from *P. putida* HK5, has been shown to be an efficient intermolecular electron acceptor from ADH IIB, and the interaction between the

[4]Correspondence: mathews@biochem.wustl.edu
[5]Present address: Center for Advanced Microstructures and Devices, 6980 Jefferson Highway, Baton Rouge, Louisiana 70806.

Key words: alcohol dehydrogenase; electron transfer; oxidation-reduction; pyrroloquinoline quinone; quinohemoprotein; X-ray crystallography

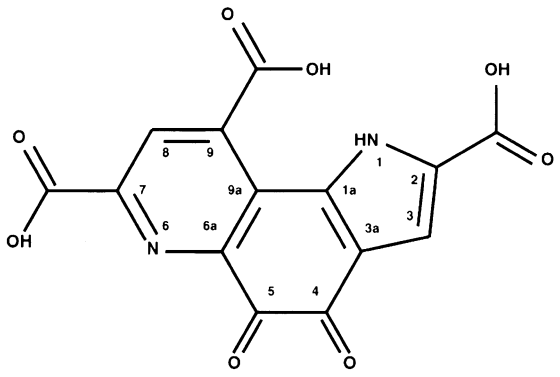

Figure 1. Chemical Structure of Pyrroloquinoline Quinone

two proteins has been shown to be a freely reversible bimolecular reaction, which is mediated largely by hydrophobic interactions between them [11]. The reduced azurin then transfers electrons to the membrane-bound cytochrome oxidase (our unpublished data).

The crystal structures of four non-heme PQQ-containing quinoproteins have been determined. Two of these are MDHs isolated from methylotrophic bacteria [12, 13], and the third is a type I ADH (ADH I), specific for ethanol, obtained from *Pseudomonas aeruginosa* [10]. The fourth is a soluble glucose dehydrogenase (GDH) isolated from *Acinetobacter calcoaceticus* [14]. In all four enzymes, the PQQ is bound to a subunit having a β propeller motif [15] in which the PQQ is located in a funnel on the central axis of the propeller. However, in MDH and ADH I the, β propeller consists of eight 4-stranded antiparallel β sheet propeller "blades" arranged around an axis of 8-fold pseudosymmetry. In GDH, the β propeller contains only six propeller blades. Furthermore, the orientation of the PQQ in GDH is the reverse of that found in MDH and in ADH I [16]. The ADH I structure is very similar to that of MDH, except that it lacks a small subunit (~8 kDa) of unknown function found in MDH. In both enzymes, the approximately planar PQQ cofactor is sandwiched between a tryptophan side chain and a characteristic disulfide bridge, composed from a pair of adjacent cysteine residues, and it forms hydrogen bonds in its equatorial plane with surrounding protein residues.

Recently, the structure of a fifth PQQ-containing enzyme, a type II quinohemoprotein ADH from *Comamonas testosteroni* (ADHCT), has been reported [17]. In addition, two new quinohemoprotein amine dehydrogenases have recently been described [18, 19]. However, these latter two enzymes do not contain PQQ, but rather a new quinone-containing cofactor, cysteine tryptophylquinone.

In this paper we report the three dimensional structure of ADH IIB at 1.9 Å resolution based on an amino acid sequence derived from the genomic DNA isolated from the bacterium and amplified by the polymerase chain reaction (PCR). The enzyme consists of a 60 kDa β propeller domain and a 10 kDa cytochrome domain, each containing the PQQ and heme moieties, respectively. Structural features relating to substrate specificity, catalytic activity, and electron transfer between PQQ and heme, as well as from heme to the putative exogenous azurin electron acceptor, are discussed. A brief comparison of the ADH IIB structure to that of ADHCT [17], which appeared after submission of this manuscript for publication, is also presented.

Results and Discussion

Cloning of the Gene Encoding ADH IIB

The structural gene of ADH IIB was cloned and sequenced by using several PCR techniques (our unpublished data). The structural gene was determined to have 2073 base pairs encoding 690 amino acid residues (Figure 2). The N-terminal amino acid sequence of the purified enzyme was determined to be AGVDEAAIRATEQA by automated sequence analysis and is completely identical to the deduced amino acid sequence starting at position 23 (Figure 2), indicating that the first 22 residues consist of a signal sequence targeted to the periplasm. The molecular mass of the mature protein (lacking the putative signal sequence) was calculated as 72,603 Da.

Amino Acid Sequence

A search of the protein sequence database using the program BLAST [20] has shown that 21 other proteins have significant sequence identity with ADH IIB. Representative sequences are shown in Figure 2. The closest in sequence to ADH IIB is a type II ADH from *Pseudomonas stutzeri* reported by Chen and colleagues (PDB Accession Number AAG09249), which shares 73% identity in 690 amino acid residues. The next closest are two type II alcohol dehydrogenases, tetrahydrofurfuryl alcohol dehydrogenase (THFA-DH) from *Ralstonia eutropha* [8] and ethanol dehydrogenase from *C. testosteroni* [6], which are 49% and 52% identical, respectively, in ~670 residues. The third closest are the quinohemoprotein subunits of five membrane-bound type III ADHs from acetic acid bacteria. These share ~44% sequence identity over ~715 amino acids. The remaining proteins are non-heme-containing type I ethanol dehydrogenase from *P. aeruginosa* and methanol dehydrogenase from various methylotrophic bacteria. They range from 37% to 33% identical in sequence over 532–624 amino acid residues.

These sequence relations indicate that the two *Pseudomonas* enzymes are closely similar and are likely to be nearly identical in structure. The greater sequence disparity with the *Ralstonia* and *Comamonas* enzymes suggests that they are less closely related structurally, to the same approximate extent as the membrane-bound type III ADHs from acetic acid bacteria. The sequence conservation within the quinoprotein domains is considerably greater than within the cytochrome domain. Although the cytochrome domains of the two *Pseudomonas* enzymes are ~58% identical to each other, those of the type III, the *Ralstonia*, and the *Comamonas* enzymes are considerably more divergent, having ~30% identity. However, the presence of the hemoprotein domain does indicate considerable evolutionary relatedness among these quinohemoproteins, since the respective quinoprotein domains retain roughly 55%–60% identity, nearly twice that with the quinoprotein domains

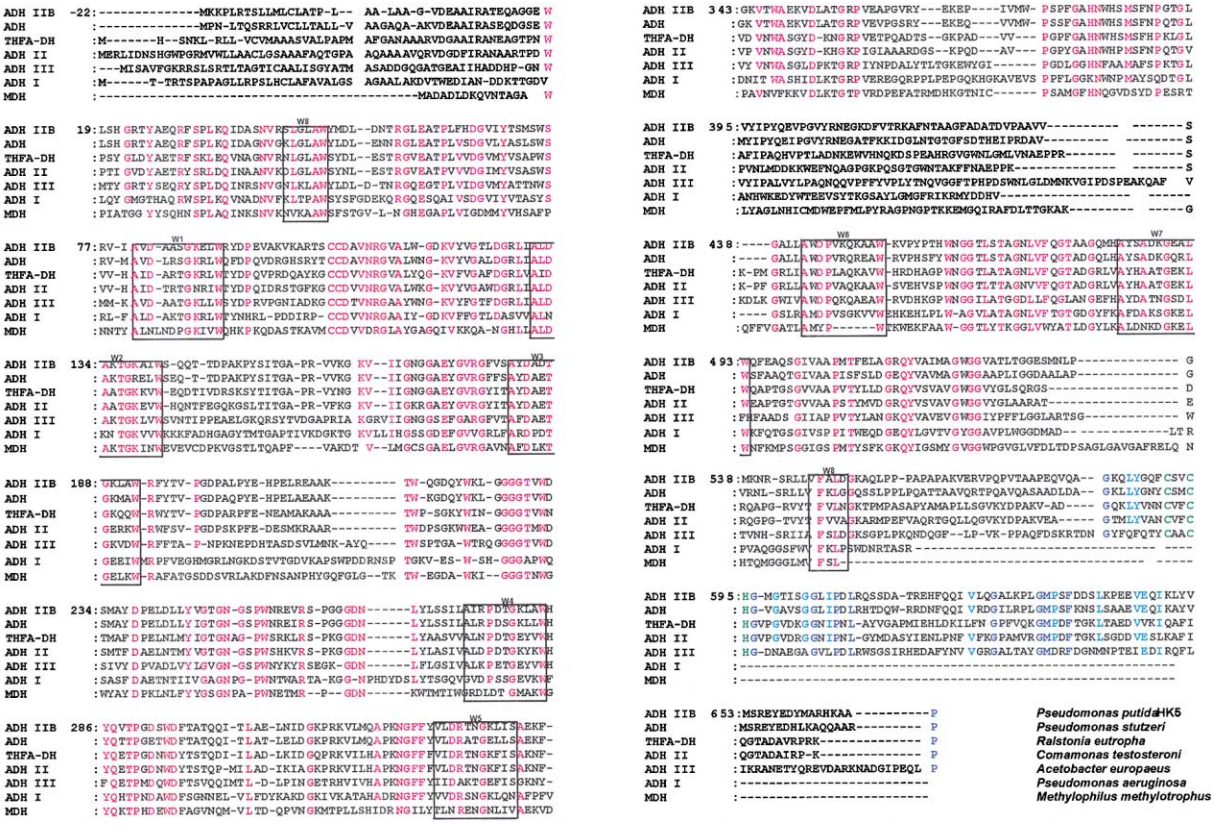

Figure 2. Sequence Comparison of ADH IIB with Representatives of Four Groups of Quinoprotein ADHs Arranged in Decreasing Order of Sequence Identity

The highest degree of identity (73%) is found for ADH from *P. stutzeri* (Accession No. AAG09249). The next group comprises THFA-DH and ADH II of *R. Eutropha* [9] and *C. testosteroni* [6], respectively (~50%). The third group is represented by ADH III from *Acetobacter europaeus* (Accession No. Q44002) (~44%), and the fourth by the non-heme quninoproteins ADH I [4] and MDH [12] from *P. aeruginosa* and *M. methylotrophus* W3A1, respectively (~35%). Boxed residues labeled "W1" to "W8" contain the "tryptophan docking motif" characteristic of the family of quinoprotein ADHs. Residues highlighted in red are identical in at least six of the seven quinoprotein domains; those highlighted in green form the heme binding motif. Residues in dark blue are identical, and those in light blue are highly conserved in sequence within the cytochrome domains.

of the ethanol and methanol dehydrogenases lacking the hemoprotein domain.

Description of the Molecule

ADH IIB consists of two domains, a 555 residue PQQ-containing N-terminal domain (residues 1–555) and an 88 residue C-terminal c-type cytochrome domain (residues 577–664) (Figure 3A). The two domains are connected by a proline-rich linker segment of 21 residues (residues 556–576), seven of which make no contact with either domain. The PQQ domain is well ordered, having an average temperature factor of 18 Å^2, while the cytochrome domain is less well ordered, with $<B> = 26$ Å^2. The linker segment is poorly ordered, with $<B> = 44$ Å^2.

PQQ Domain

The PQQ domain of ADH IIB forms an 8-bladed β propeller very similar in structure to the methanol dehydrogenase (MDH) from *Methylophilus methylotrophus* W3A1 [12] with which it shares ~33% sequence identity overall. The root mean square deviation (rmsd) of 469 equivalent Cα positions in the two structures is 1.16 Å, and the matched residues show 37% sequence identity. Comparison of ADH I with ADH IIB shows that these two proteins have slightly closer similarity, with 481 matched residues displaying 1.08 Å rmsd and 41% sequence identity. There are five segments showing large structural differences between ADH IIB and MDH (Figure 3B). The first segment (labeled S1 in Figure 3B) is found at the amino terminus. Segments 2 and 3 are located in connecting loops between propeller blades, one between blades 3 and 4 and the other between blades 5 and 6; segments 4 and 5 are located in loops between strands 2 and 3 of propeller blades 6 and 8, respectively. Four of these segments (all but the first) also show large deviations between ADH IIB and ADH I. The structural deviation of segment 1 appears to play no obvious functional role, nor do those of segments 2 and 3, although they may be linked to the presence of the small β subunit of MDH. On the other hand, the large deviations of segments 4 and 5 are probably related to the presence of the cytochrome domain in ADH IIB, since portions of segments 4 and 5 of ADH IIB appear to interact favorably

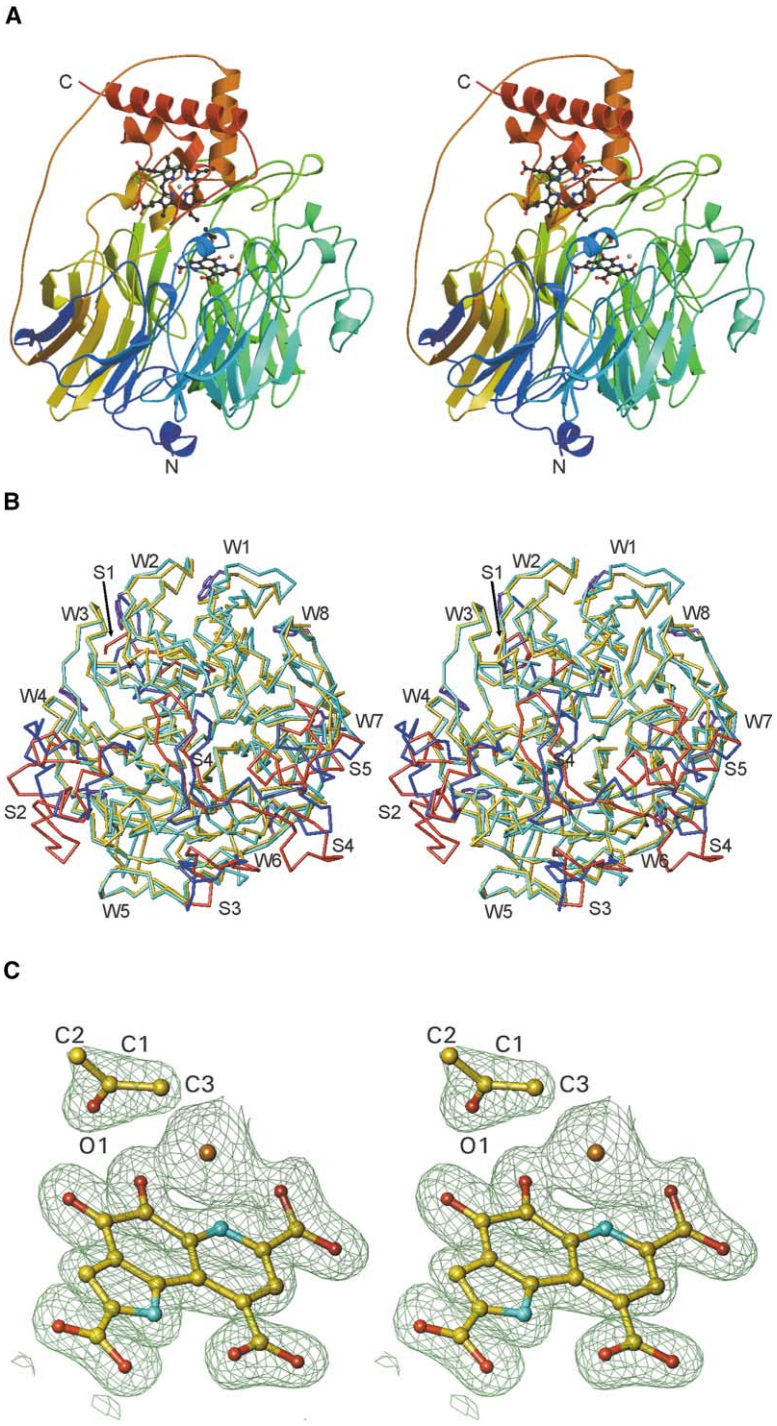

Figure 3. Stereo Diagrams of ADH IIB, Its Comparison with MDH, and the Electron Density of PQQ

(A) Ribbon diagram of ADH IIB. The color of the ribbon ramps from dark blue at the N terminus through green, yellow, and orange to red at the C terminus. Ball-and-stick figures for the heme, PQQ, calcium, and acetone are drawn with carbon = black, oxygen = red, nitrogen = blue, calcium = gray, and iron = gray. This diagram was made using MOLSCRIPT [53] and RASTER3D [54].

(B) Comparison of the quinoprotein domain of ADH IIB with the α subunit of MDH from *M. methylotrophus* W3A1. MDH is yellow and ADH IIB is green where the two chains are closely similar. Where the two chains diverge significantly, MDH is blue and ADH IIB is red. The eight blades of the β propeller are labeled W1-W8. The five polypeptide segments where the chains diverge significantly are labeled S1-S5; segment S4 extends from the edge to the center of the propeller and is labeled in both regions. The seven conserved tryptophan residues in the outer strand of each blade of ADH IIB (all but blade 5) are shown in purple.

(C) Electron density of the PQQ, calcium, and acetone molecules of ADH IIB. The density was computed using coefficients (2Fo-Fc) and contoured at 1.25 σ where Fo and Fc are the observed and calculated structure factors, and σ is the root mean square value of the electron density. Except where noted, this and subsequent diagrams were made using TURBO-FRODO [48].

with its cytochrome domain while segment 5 in MDH would clash with the cytochrome domain. The binding site for the second α subunit of MDH is not close to any of the deviating segments with respect to ADH IIB. However, the linker between the propeller and cytochrome domains of ADH IIB would pass through the second MDH subunit. Despite this, however, there appears to be no interference between the cytochrome domain of ADH IIB and the second MDH subunit, suggesting that the electron acceptor for MDH, cytochrome c_L, might bind to the MDH heterotetramer in a similar way and that the ADH IIB molecule could serve as a good model for the MDH/CytC_L interaction.

The PQQ (Figure 1) is bound near one end of the β propeller of ADH IIB near the 8-fold axis of pseudosymmetry (Figure 3A). The PQQ ring is essentially planar (Figure 3C). Its environment is very similar to that of PQQ in MDH and ADH I. It is sandwiched between the side chains of Trp232 below it and a vicinal disulfide bridge connecting Cys105 and Cys106 above it, making

van der Waals contact at both surfaces. A calcium ion is tightly bound to PQQ (Figure 3C), being coordinated to ring atoms O-5, N-6, and a carboxylate oxygen, O-7a; the pyrrole nitrogen N-1 forms an intramolecular hydrogen bond to the carboxylate oxygen, O-9b.

The calcium ion, as well as the six carboxylate oxygen atoms and two quinone oxygens of PQQ (Figure 1), forms electrostatic and hydrogen bonding interactions with several protein main and side chain atoms. The three major differences between the PQQ interactions with ADH IIB and with MDH and ADH I are the positionally equivalent substitution of Lys322 by Arg (at O-4 and O-5) and of Gly170 by Ser (at O-9a) in MDH and ADH I and the positionally nonequivalent replacements of Trp383 by a different Trp in MDH and ADH I (at O-2B). In addition, the side chain of Asn250 in ADH IIB is hydrogen bonded to O-7a, but the equivalent asparagines in MDH and ADH I are not. ADH I also differs from both ADH IIB and MDH by its interactions of O-7a and O-7b of PQQ with Asp178 and Gly177.

A repeating pattern of 7 tryptophan residues, each at the same location in the outer strand of seven of the eight propeller blades, is observed in ADH IIB (Figure 3B). This pattern is associated with a partially conserved "tryptophan docking motif" that is also found in MDH [12, 13] and in ADH I [10] (as well as in ADHCT [17]) that interlocks five of the eight adjacent pairs of propeller blades. This motif is contained within a block of 11 residues in each propeller blade that usually contains Ala, Gly, and Trp at positions 1, 7, and 11 (Figure 2) and probably helps stabilize the structure of the 8-bladed β propeller.

Cytochrome Domain

The cytochrome domain contains three α helices that make up 40% of the domain. The first α helix, about 5 turns in length, starts at Pro577 and extends to His595, the first heme ligand. The second α helix, about 3 1/2 turns in length, begins at Asp613 and ends at Gln625, 8 residues before the second heme ligand, Met633. The third α helix, nearly 6 turns in length, extends from Pro642 to Ala662, near the end of the molecule. The first and third α helices pack against each other at an angle of about 80°, a structural feature characteristic of c-type cytochromes [21]. There are also two very short 3_{10} helices, one immediately following the first α helix and the other about 3 residues beyond the second α helix, but no other secondary structure.

The heme group is inserted into a hydrophobic pocket formed by the three helices and an extended chain. The heme group is covalently attached to the domain through two thioether linkages from Cys591 and Cys594 to the vinyl methylene carbons CAB and CAC, respectively. Although most of the heme group is buried in the interior of the enzyme, the two propionic acid groups are exposed to solvent.

In a search of known protein structures using the program DALI [22], 11 cytochromes were identified as similar in structure to the ADH IIB cytochrome (A2B-Cyt) domain. This result was based on a composite score (Z score from 8.8 to 4.7) that ranks the degree of structural similarity in standard deviation units; the first noncytochrome structure had a Z score of 2.3. The A2B-Cyt domain and the six most similar structures (with Z scores between 8.8 and 6.6) are compared in Table 1. The cytochrome most similar to the A2B-Cyt domain is the 78 residue cytochrome subunit of *p*-cresol methylhydroxylase (PCMH) from *P. putida* (PCMH-Cyt) (Figure 4A) [23]. It, along with cytochrome c_{551i} from *P. denitrificans* (Cyt-C551I) [24], also contains three α helices in the cytochrome core structure. They show the smallest rmsd of equivalent Cα atoms (1.1 Å and 1.3 Å, respectively, compared to 1.5–1.6 Å for the remainder) and are among the highest in sequence identity of matched residues. The A2B-Cyt domain and PCMH-Cyt also have both propionic acids of their heme groups exposed to solvent. Of the other cytochrome molecules or domains, three (Cyt-C551I, cytochrome c_6 (Cyt-C6) [25], and cytochrome c_{552} (CytC-552) [26]) have only one propionate (at position D) exposed to solvent while the remainder have neither propionic acid group exposed. ADH IIB and PCMH are both isolated from *P. putida*, and both utilize azurin as a soluble electron acceptor protein [11, 27]. Cyt-C6 and Cyt-C552 and the two domains of the flavocytochrome c sulfide dehydrogenase cytochrome (FCSD-Cyt1 and FCSD-Cyt2) subunit [28] have four α helices in the core cytochrome domain. Three are common to the three α helices in A2B-Cyt, PCMH-Cyt, and CytC-551I, while the fourth helix is located in different chain segments in Cyt-C6 and Cyt-C552 compared to the two FCSD-Cyt domains. The last cytochrome in Table 1, yeast cytochrome c isozyme 1 (Cyt-CYI1) [29], is of mitochondrial origin and contains five helices in the core cytochrome domain. Three are common to the other cytochromes, while the remaining two are in different segments from any of the four-helix cytochromes.

Ligand Binding and Catalysis

ADH IIB was crystallized in the presence of isopropanol, a substrate for the enzyme [5]. As a consequence, the heme group is expected to be in the reduced form. This has been verified by polarized single-crystal absorption microspectrophotometry (A. Merli, personal communication). During the final stages of model building, a flat piece of positive density in the (Fo-Fc) difference map was found in the active site that could be modeled as acetone, the oxidation product of isopropanol, and was subsequently refined. Its keto oxygen position was consistent with the electron density (Figure 3C) and with its close interaction (2.6–3.0 Å) with O-4 and O-5 of PQQ and with a carboxylate oxygen of Asp295. The remainder of the acetone molecule is directed away from the PQQ into a cavity lined almost exclusively by hydrophobic side chains (Figure 4B). These side chains consist of three phenylalanines, two cysteines, one tryptophan, one proline, and one valine, as well as PQQ. The volume of the substrate cavity is about 120 $Å^3$ and appears to be about two to three times larger than the volume of the acetone molecule, providing a structural basis for the rather broad substrate specificity for 4–8 chain primary and secondary alcohols and diols.

The mouth of the channel leading to the active site cavity is composed of two segments from the PQQ binding domain, residues 403–406 and residues 424–435

Table 1. Structural Comparison of the ADH IIB Cytochrome Domain with Six Other Similar C-Type Cytochromes

Protein[a]	A2B-Cyt	PCMH-Cyt	Cyt-C551I	Cyt-C6	Cyt-C552	FCSD-Cyt1	FCSD-Cyt2	Cyt-CYI1
PDB code	1KV9	1DII	2MTA	1CTJ	1C52	1FCD	1FCD	1YCC
Z score[b]	21.0	7.5	8.1	8.8	6.9	6.6	–	6.7
Total residues	88	73	147	89	131	83	91	108
Core cytochrome[c]	577–659	6–74	43–124	3–87	3–92	3–77	88–173	2–103
Number of helices in core	3	3	3	4	4	4	4	5
Sequence identity (%)[d]	–	25	20	18	25	14	–	15
Number of equivalent residues[e]	–	54	65	61	61	55	49	56
Number of fragments[e]		5	4	4	6	5	4	5
Rmsd (Å)[e]	–	1.13	1.33	1.58	1.58	1.61	1.52	1.51
Number of identical residues[e]	–	19	17	14	17	10	9	10
Identically matched (%)[e]	–	35	26	23	27	18	18	18
Exposed propionates	both	both	D only	D only	D only	none	none	none

[a] Abbreviations: A2B-Cyt, cytochrome domain of ADH IIB; PCMH-Cyt, cytochrome subunit of PCMH [23]; Cyt-C551I, cytochrome c_{551i} from *P. denitrificans* [24]; Cyt-C6, cytochrome c_6 from *Monraphidium Braunii* [25]; Cyt-C552, cytochrome c_{552} from *Thermus thermophihlus* [26]; FCSD-Cyt1, first cytochrome domain of the diheme cytochrome subunit of flavocytochrome c sulfide dehydrogenase (FCSD) [28]; FCSD-Cyt2, second cytochrome domain of the diheme cytochrome subunit of FCSD; Cyt-CYI1, isozyme 1 of mitochondrial cytochrome c from *Saccharomyces cerevisiae* [29].

[b] Strength of the structural similarity in standard deviations above expected, as defined by the DALI server [22]. This quantity was not calculated for FCSD-Cyt2.

[c] The core cytochrome extends approximately from the start of the helix just before the CXXCH motif to the end of the helix following the methionine ligand.

[d] The overall sequence identity was computed using the DALI server [22]. This quantity was not calculated for FCSD-Cyt2.

[e] Computed using LSQMAN [51].

(Figure 4C). The latter segment is partially in contact with the cytochrome domain and is contained within segment S4 (residues 409–437) of ADH IIB, which differs significantly in conformation from a corresponding segment in MDH (see Figure 3B). The active site cavity is blocked from bulk solvent within the channel by the side chains of Phe378 and Phe425, which partially line the entrance channel. Movement of either of these side chains would facilitate substrate binding and interchange with product.

In MDH [30], the active site cavity is small, having a volume of ~18 Å^3. The active site cavity of ADH I [10] is larger, with a volume of ~62 Å^3. Examination of the ADH IIB active site cavity (~120 Å^3) with MDH and ADH I superimposed shows that Trp531 of MDH bisects the ADH IIB cavity, sterically blocking acetone binding, and that Leu547 brushes the cavity surface, further reducing the usable volume in MDH (Figure 5A). Trp531 was noted by Keitel et al. [10] as limiting the MDH active site volume when compared to ADH I, and in ADH IIB, Trp531 is replaced by Pro377 and Phe378. In ADH I, three side chains lie in close proximity to the ADH IIB cavity, restricting the usable volume for substrate binding in ADH I. These are Phe408, Leu409, and Trp557 and are replaced by Pro377, Phe378, and Thr529 in ADH IIB (Figure 5A). Trp577 of ADH I is replaced by Leu547 in MDH and was predicted by Keitel et al. [10] to act as a gate in ADH I for substrate entry, based on docking experiments.

The redox potential of the heme of ADH IIB is ~+190 mV [11]. Although the PQQ redox potential in ADH IIB has not been measured, its potential in the soluble GDH has been measured [31], giving values of ~+30 mV for the reduced/semiquinone couple and ~−10 mV for the semiquinone/oxidized couple. The redox potential of PQQ bound to ADH IIB is likely to be similar. Thus, on binding to ADH IIB, isopropanol would deliver a pair of electrons to the PQQ, one of which would then be transferred to the heme, leaving the PQQ as the semiquinone. C-type cytochromes are generally resistant to oxidation by molecular oxygen, and MDH, which is functionally similar to ADH IIB, is usually isolated in the semiquinone state [2]. In fact, ADH IIB isolated in the presence of trace amounts of contaminating alcohols displays a PQQ semiquinone EPR signal (our unpublished data). The planar nature of the PQQ ring (Figure 3C) is consistent with the semiquinone form, as predicted on the basis of quantum mechanical calculations [32].

Two plausible mechanisms have been proposed for the oxidation of substrate alcohols by PQQ-containing ADHs, one involving an addition-elimination reaction with a hemiketal intermediate, and the other a direct hydride transfer from the C-1 of the substrate to PQQ [33]. Both mechanisms involve base catalysis in the first step for removal of the proton of the O-1 hydroxyl group. The carboxylate group of Asp295 in ADH IIB, to which the keto oxygen of acetone is hydrogen bonded, is the closest nucleophile to the active site cavity that could serve this function.

The next step in the reaction would be either a hydride transfer from substrate C-1 to C-5 of PQQ or the transient formation of a covalent bond between C-5 and substrate O-1 to form a hemiketal intermediate. If isopropanol is modeled into the active site of ADH IIB so as to be nearly coincident with the acetone, the O-1 atom of isopropanol is about 3.4 Å from C-5 of PQQ, and the C-1 atom is about 4.1 Å from C-5. Hemiketal formation would require some reorientation of the substrate; however, there are no apparent steric constraints preventing that from happening. Likewise, the expected position for the methylene hydrogen of isopropanol is not very well oriented for hydride transfer, although the distance and angle can also be improved for hydride transfer by rotation of the isopropanol model about the O-1 atom without disrupting the active site geometry. Thus, the location of the acetone product molecule does not seem to favor one mechanism for catalysis over the other.

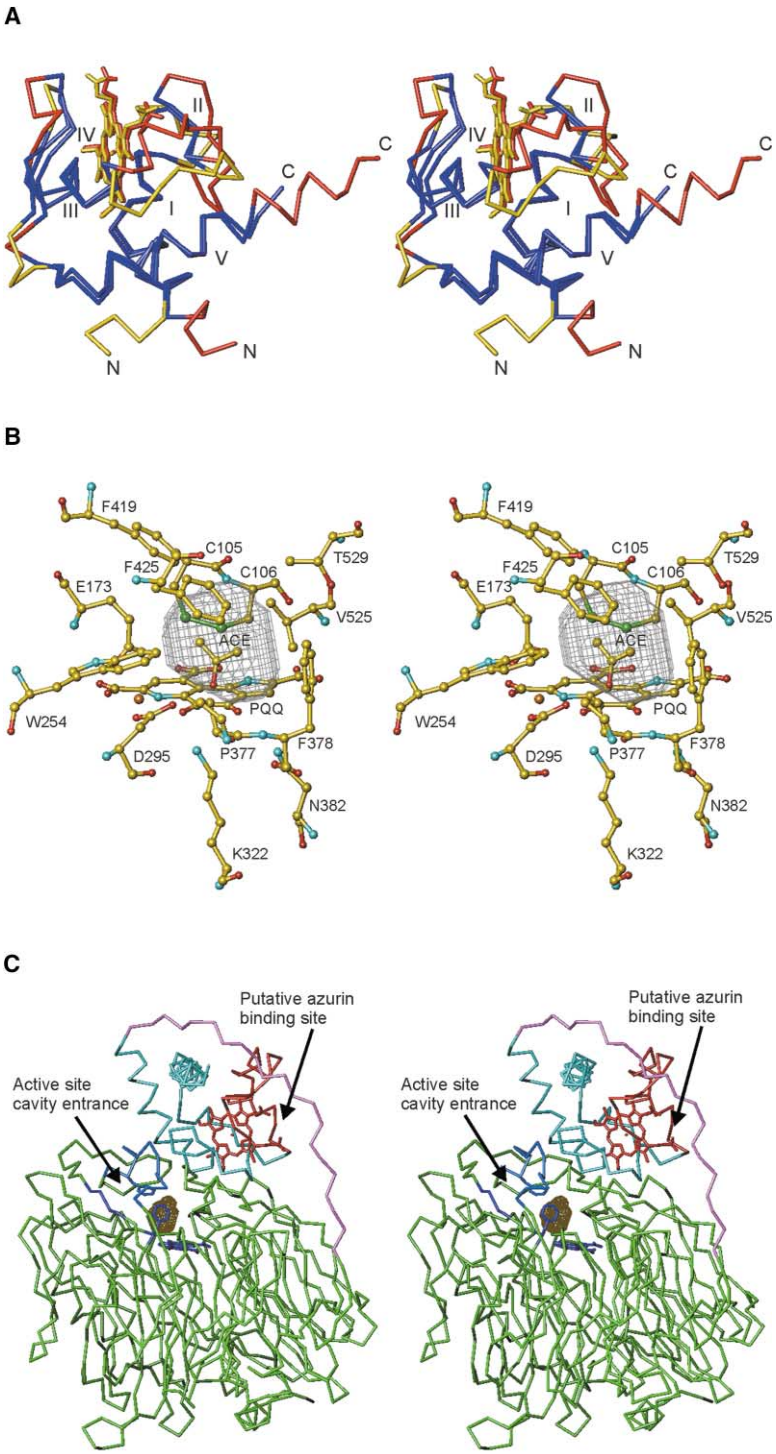

Figure 4. Stereo Diagrams of the Cytochrome Domain, the Active Site Cavity, and the Putative Azurin Binding Site

(A) Comparison of the cytochrome domain of ADH IIB (residues 577–664) with the cytochrome subunit of *p*-cresol methylhydroxylase (PCMH). The five peptide fragments of high structural homology, indicated by roman numerals, are in blue, and the intervening segments of low structural homology as well as the heme groups are in red for ADH IIB and in yellow for PCMH.

(B) Active site cavity of ADH IIB shown with chicken wire representation and containing the reaction product, acetone. The PQQ and the 13 side chains, mostly hydrophobic, of the quinoprotein domain that surround and help form the cavity are labeled.

(C) Cα tracing of ADH IIB showing the active site cavity entrance and putative azurin binding site. The quinoprotein and cytochrome domains are green and azure, respectively, and the linker segment is violet. The residues lining the cavity (403–406 and 424–435) are blue, and the residues partially surrounding the putative azurin binding site (605–631) plus the heme are red. The cavity is represented as chicken wire, and the side chains separating the cavity from solvent, Phe378 and Phe425, as well as PQQ are also in blue.

Comparison with Glucose Dehydrogenase

In GDH, a hydride transfer mechanism has been firmly established for oxidation of the C-1 atom of glucose [14, 33, 34] and has been postulated for MDH [30, 35, 36]. In GDH, the O-1 of bound glucose is hydrogen bonded to an active site histidine, which could act as a base to abstract the hydroxyl proton. Glucose binding is also stabilized by hydrogen bonding of O-1 to the side chains of two other residues, a glutamine and an arginine. The C-1 atom is 3.2 Å from the C-5 atoms of PQQ and oriented optimally for transfer of a hydride ion, but unfavorably for the addition-elimination reaction.

Figure 5B shows the PQQ moiety of GDH, along with the glucose and the histidine and arginine side chains hydrogen bonded to it, superimposed upon the active site of ADH IIB. To do this superposition, it was first necessary to reflect the coordinates of these groups through the plane of the PQQ, since PQQ binding to the β propeller of GDH is the reverse of that in ADH IIB [14]. Isopropanol was then modeled onto the C-1, O-1, C-2,

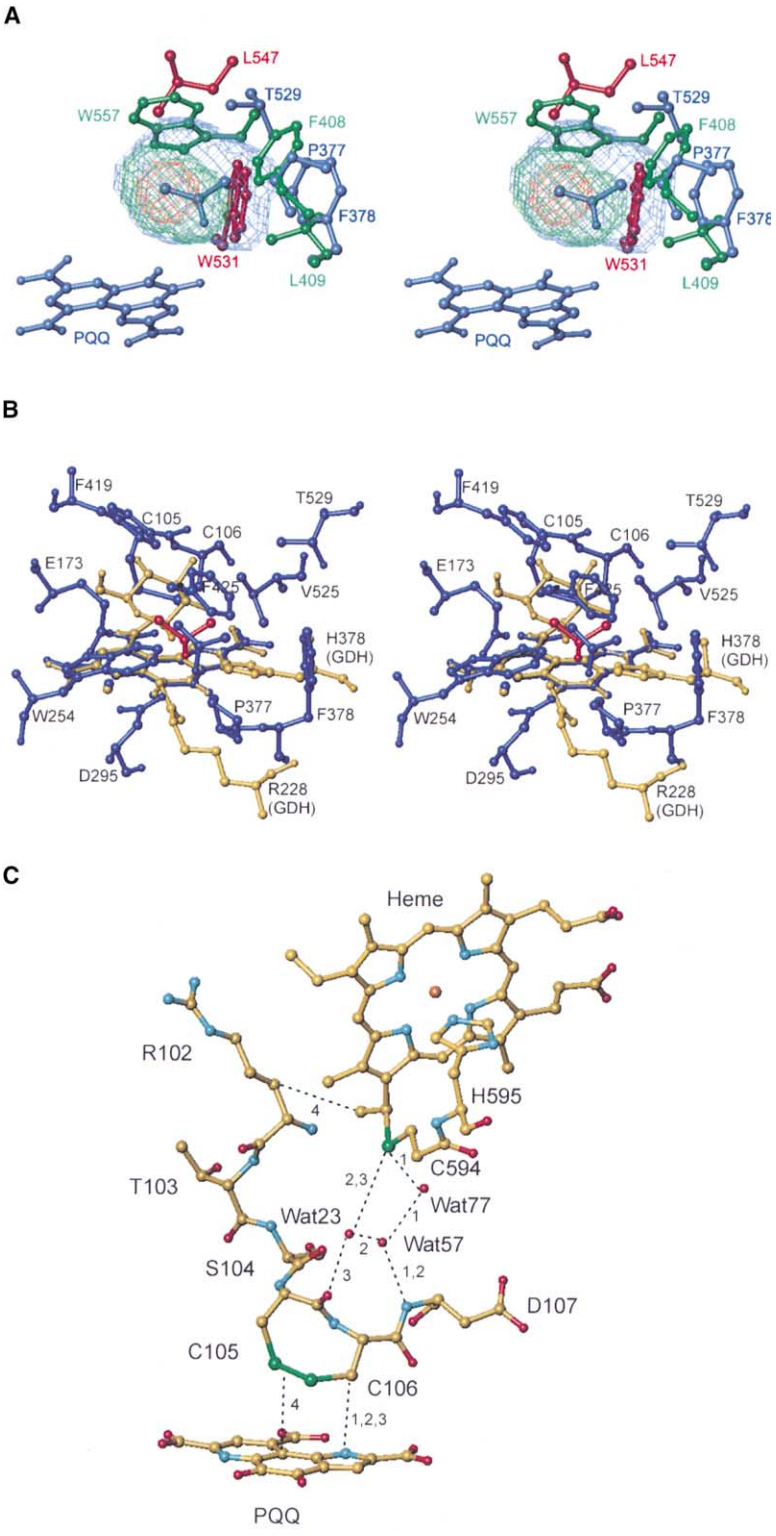

Figure 5. Comparisons of Active Sites as Well as the Arrangement of Redox Cofactors in ADH IIB

(A) Active site cavities of ADH IIB (blue), ADH I (green), and MDH (red) with side chains that limit access to the cavity in each of the proteins: Trp531 and Leu547 in MDH (red); Phe408, Leu409, and Trp557 in ADH I (green); and the replacement side chains Pro377, Phe378, and Thr529 in ADH IIB (blue).

(B) Active site of ADH IIB (blue) with the PQQ moiety, glucose substrate, and two interacting side chains of GDH (yellow) superimposed after reflection of the GDH groups through the PQQ plane as described in the text. A hypothetical model of isopropanol that was manually adjusted in position to minimize bad contacts with the ADH IIB side chains is shown in red.

(C) The four most likely pathways for electron flow from atom C-5 of PQQ to the heme iron as predicted by the program GREENPATH 0.97 [38]. Paths 1–3 involve electron flow through water molecules while path 4 does not (see text).

and O-5 atoms of glucose to simulate a binding mode to the enzyme that might be favorable to hydride transfer in ADH IIB. However, the C-2 and C-3 atoms of isopropanol made close contact to the sulfur atoms of Cys105 and Cys106 and to the side chain of Glu173, a calcium ligand; also, the O-1 atom could not form a hydrogen bond to the side chain of Asp295 as observed in the binding of acetone. Small manual adjustments of the modeled isopropanol could remove some of the strain and allow the hydrogen bond between O-1 and Asp295 to form, possibly leading to stable binding suitable for hydride ion transfer (Figure 5B).

Table 2. Direct Ionic and Hydrogen-Bonded Interactions between the Quinoprotein and Cytochrome Domains of ADH IIB

PQQ Domain	Cyt Domain	Distance (Å)
Arg102 NH2	Asp638 OD1	3.0
Arg102 NH1	Asp638 OD2	3.1
Asn535 OD1	Ser601 O	2.9
Thr529 O	Met597 N	2.7
Gly531 N	Ile600 O	3.0

PQQ and Heme Domain Interaction and Electron Transfer

The cytochrome domain of ADH IIB sits above the β propeller domain approximately coincident with its 8-fold pseudosymmetry axis (Figure 3A). The heme group is somewhat displaced from the pseudosymmetry axis, with helix 1 of the cytochrome domain occupying the top of the funnel instead. The total surface area of the two domains that is buried in the complex is about 2200 Å^2, or about 1100 Å^2 per domain, ignoring any effect of the linker region. The two domains are linked by one salt bridge pair of hydrogen bonds and three additional hydrogen bonds, one between a main chain and side chain atom and two between pairs of main chain atoms (Table 2). In addition, there are 13 bridging water molecules in the interface that form one or more hydrogen bonds with both domains as well as with additional water molecules (Table 3). The iron atom of the heme and the C-5 atom of PQQ are separated by 20.6 Å, and the planes of the two groups are tilted to each other by about 70°. The distance between the two conjugated rings is about 15 Å.

In a weakly coupled electron transfer system, the rate of electron transfer between a donor (D) and an acceptor (A) group can be written as

$$k_{ET} \propto (2\pi/\hbar)|T_{DA}|^2(\text{F.C.}),$$

where $\hbar$ is Plank's constant, (F.C.) is the Franck-Condon nuclear tunneling factor, and T_{DA} is the electronic tunneling coupling matrix element between donor and acceptor [37]. This coupling can be estimated from the length of the path along chemical bonds and between nonbonded atoms that link the donor and acceptor. The PQQ and heme group are separated by a covalent chain of five amino acids, residues 102–106, as well as by several water molecules that could provide paths for electron flow along the bonds connecting the atoms between the two prosthetic groups (Figure 5C). According to calculations using GREENPATH 0.97 [38], the most efficient path for electron flow from the C-5 of PQQ to the heme iron involves a through-space jump from the N-1 of PQQ to Cys106 Cβ, travel through the amide nitrogen of Asp107 and along hydrogen bonds through waters #57 and #77, followed by a through-space jump to Sγ of Cys594 and then to the heme ring (path 1); the resulting relative electronic coupling is $1.0 \cdot 10^{-6}$. Removal of water #77 from the calculation leads to recruitment of water #23 instead (path 2) and a drop in the relative coupling to $2.6 \cdot 10^{-7}$; removal of both waters #57 and #77 results in utilization of water #23 alone, but via the carbonyl oxygen of Cys105 (path 3), and leads to a relative coupling of $2.3 \cdot 10^{-7}$. Elimination of all three waters causes a new path to be invoked (path 4) involving a jump from C-9a of PQQ to the disulfide bond of Cys105-Cys106, travel along side and main chain atoms to the Cα of Arg102, followed by a jump to the heme ring; this path leads to a relative coupling of $1.2 \cdot 10^{-7}$, 8-fold lower than the best coupling involving hydrogen bonded water molecules.

The four pathways for through-bond coupling delineated above (Figure 5C) all include Cys105 and/or Cys106 that form a disulfide bridge as part of the path. The equivalent vicinal disulfide in MDH was proposed to be involved in the electron transfer from PQQ to cytochrome c_L in MDH during its oxidative half reaction [39]. It was subsequently shown that carboxymethylation of these two cysteines did not interfere with heme reduction by reduced MDH [40], suggesting that the disulfide bridge is not required for electron transfer. However, only path 4 above specifically utilizes the disulfide bridge, while the other three paths involve Cys106 only. Furthermore, this electron transfer step in ADH IIB is intramolecular, to the heme c moiety directly above the disulfide, rather than intermolecular, to an exogenous cytochrome as in the case of MDH/cytochrome c_L. The

Table 3. Water Molecules that Mediate Hydrogen Bonding Interactions between the Quinoprotein and Cytochrome Domains of ADH IIB

Water[a]	Residue 1	Distance (Å)	Residue 2	Distance (Å)	Residue 3	Distance (Å)	Water[b]	Water[b]
15	W522 NE2	2.7	M534 O	2.8	G602 O	2.7	–	–
43	F419 N	2.9	Q589 O	2.9	–	–	145	491
66	T527 O	2.7	L604 N	2.9	–	–	96	–
77	R56 NH2	2.8	C594 SG	3.3	–	–	57	123
96	L528 O	2.7	C594 O	2.8	G602 N	3.0	66	–
105	K98 O	2.8	G632 O	2.8	–	–	123	289
111	M539 O	2.8	G602 O	2.8	–	–	74	
116	F419 O	2.8	Q589 O	2.7	–	–	147	459
125	K417 N	2.9	S639 OG	2.8	–	–	535	–
221	T429 O	2.8	R655 NH2	2.9	–	–	–	–
272	V99 N	3.1	K629 O	2.9	–	–	243	710
363	T55 O	2.8	L604 O	2.7	–	–	206	–
531	D427 O	2.7	K584 NZ	3.2	–	–	–	–

[a] The primary bridging water molecule.
[b] Secondary water molecules that are also hydrogen bonded to the primary mediating waters.

Table 4. Data Collection and Refinement Statistics

Data Collection							
Data set	Native	U1	Hg1	U2p	U2e	U2h	Hg2p
Wavelength (Å)	1.5418	1.5418	1.5418	0.72158	0.72185	0.69723	1.00760
Resolution	1.9	2.2	2.2	2.0	2.0	2.0	2.45
Number of unique reflections	48,675	30,171	31,835	46,952	46,882	46,905	24,994
Average multiplicity	3.5	1.7	2.0	3.4	3.4	3.5	3.3
Completeness[b] (%)	87.1 (47.3)	83.9 (47.5)	88.5 (53.9)	96.5 (90.3)	96.2 (88.7)	96.7 (92.7)	95.9 (93.2)
R_{merge}[c] (%)	6.4 (21.5)	7.6 (13.1)	8.0 (14.9)	5.9 (11.9)	5.5 (10.3)	6.1 (9.9)	3.5 (5.7)
$<I/\sigma(I)>$[d]	18.2 (4.2)	9.0 (4.0)	10.7 (5.0)	19.0 (7.6)	20.5 (9.0)	20.3 (10.4)	27.8 (13.2)

Phasing statistics		Model	
m[e], phase set 1[f]	0.69	Number of non-H protein atoms	5,172
m[e], phase set 2[g]	0.49	Number of solvent molecules	732
Refinement		Number of prosthetic groups	2
Resolution range (Å)	30–1.9	Number of calcium ions	1
Number of reflections	48,672	Number of additional molecules	3
Working set	43,750	Rmsd bond lengths (Å)	0.006
Test set	4,922	Rmsd bond angles (deg.)	1.44
R_{cryst}[h] (%)	15.4	Mean protein B factor (Å^2)	20.0
R_{free}[i] (%)	18.9	Mean solvent B factor (Å^2)	31.9

[a] Abbreviations: U1, uranyl acetate, home detector; Hg1, methyl mercuric chloride, home detector; U2p, uranyl acetate, APS, peak; U2e, uranyl acetate, APS, edge; U2h, uranyl acetate, APS, high; Hg2p, methyl mercuric chloride, SSRL, peak.
[b] Highest resolution shell in parentheses.
[c] $R_{merge} = \Sigma_h\Sigma_i|I(h) - I_i(h)|/\Sigma_h\Sigma_i I_i(h)$, where $I_i(h)$ is the ith measurement and I(h) is the mean measurement of reflection h.
[d] $I/\Sigma(I)$ is the average signal-to-noise ratio for merged reflection intensities.
[e] m, mean figure of merit.
[f] Phase set 1 includes data sets U1, Hg1, U2p, U2e, and U2h and was truncated at 2.5 Å resolution and improved by density modification in SHARP [45].
[g] Phase set 2 includes data sets U1, Hg1, U2p, U2e, and Hg2p and was extended to 1.9 Å resolution in SHARP [45] by density modification [45].
[h] $R = \Sigma_h|Fo - Fc|/\Sigma_h|Fo|$, where Fo and Fc are the observed and calculated structure factor amplitudes of reflection h.
[i] R_{free} is the test reflection data set; about 10% was selected randomly for crossvalidation during crystallographic refinement.

functional role of the Cys105-Cys106 disulfide will be investigated in the future by site-directed mutagenesis.

Electron Transfer from ADH IIB to Azurin

Azurin isolated from *P. putida* HK5 has been shown by in vitro steady-state kinetic analysis to be a good electron acceptor from ADH IIB, with a first order rate constant of approximately 50 s^{-1} at 25°C [11]. The apparent K_m for the reaction decreases with increasing ionic strength, indicating that the interaction of the two proteins is mediated by hydrophobic forces. In azurin, one of the histidine ligands to the buried copper atom is exposed to solvent and is surrounded by a surface patch of hydrophobic residues. In ADH IIB, the heme group is buried within the cytochrome domain, except for the propionic acid-containing edge of the heme, which is exposed to solvent. This edge is partially surrounded by a polypeptide segment consisting of residues 605–631 of the cytochrome domain that could form a putative azurin binding site (Figure 4C). The electrostatic potential of this putative binding surface, computed with the program GRASP [41], exhibits a distinct negative region, centered on the exposed propionic acid groups, that is surrounded by a charge-neutral surface formed by the 605–631 segment. The interaction of azurin with ADH IIB mediated through these charge neutral regions would be consistent with the observed ionic strength dependence of the reaction. A similar interaction between the Rieske iron-sulfur cluster subunit with the heme propionate-containing region of cytochrome c_1 in the bc_1 complex [42] has been reported.

Comparison with ADHCT

The recently reported crystal structure of ADHCT [17] appears to be very similar to that of ADH IIB. The overall rms deviation for 576 equivalent Cα atoms is 1.08 Å. For the separately aligned domains, the rms deviations are 0.85 Å for 516 equivalent quinoprotein Cα atoms and 1.28 Å for 76 equivalent cytochrome Cα atoms. The sequence identity for equivalent residues in the two types of domains are 56.8% and 31.6%, respectively. Despite the larger rms deviation for the two cytochrome domains, their folding patterns are nearly identical. Surprisingly, one of the most significant deviations in the quinoprotein structures corresponds to segment 425–435 of ADH IIB, which forms part of the mouth of the substrate entrance channel. The active site of ADHCT contains a molecule in the active site identified as the reaction product tetrahydrofuran-2-carboxylic acid.

Biological Implications

Quinoproteins, enzymes containing a quinone redox cofactor such as PQQ, have been recognized as the third most widespread class of redox enzyme following pyridine nucleotide- and flavin-dependent dehydrogenases. About 20 species of enzyme carrying PQQ or related quinone cofactors as the prosthetic group have been

identified so far. Some, called quinohemoproteins, have heme c moieties as additional prosthetic groups within a single protein molecule. ADH is the largest subgroup of quinoproteins and includes four different types of enzyme, methanol dehydrogenase (MDH), quinoprotein ADH (type I), quinohemoprotein ADH (type II), and membrane-bound quinohemoprotein ADH (type III).

Structural and functional studies of MDH, type I ADH, and other quinoproteins have revealed the unique position of quinoproteins among redox enzymes with respect to their catalytic and electron transfer properties. In addition, the unique properties of quinoproteins have also led to biotechnological applications in the fields of biosensors, bioconversion of useful compounds, and environmental treatment.

The structural elucidation of a quinohemoprotein type II ADH presented here has led to three major findings. (1) Common structural features observed previously for PQQ binding in ADHs are conserved. (2) The protein structure just above the PQQ plane can explain the unique substrate specificity for a broad range of longer alcohol substrates, compared with the narrow specificity of MDH and type I ADH for smaller substrates. (3) The structure around the heme c moiety shows possible intramolecular electron transfer paths from PQQ to heme c and possible intermolecular electron transfer interactions between heme c and azurin, an electron transfer mediator between ADH and cytochrome oxidase.

Experimental Procedures

Protein Purification

ADH IIB was isolated from extracts of *Pseudomonas putida* HK5 and purified as described previously [5].

Cloning of the Structural Gene

Two representative peptides derived by trypsin digestion of purified ADH IIB were isolated by reverse-phase HPLC. Based on the results of automated amino acid sequence analysis, two oligonucleotide primers were designed, and PCR amplification was performed using the genomic DNA purified from *P. putida* HK5 as the template. The resulting 0.44 kb product was cloned and sequenced. New primers were designed based on the nucleotide sequence, and several PCR products containing a part of the structural gene of ADH IIB were obtained. In vitro cloning was done according to the vendor's manual (LA PCR in vitro Cloning Kit [TaKaRa]), although the PCR was performed by using Ready.To.Go/PCR Beads Kit (Amersham-Pharmacia, Piscataway, NJ). Detailed results will be published elsewhere (our unpublished data).

The nucleotide sequence was determined by the chain termination method using PCR in conjunction with both universal and specific primers and analyzed by using ABI PRISM 310 (PE Biosystems). Sequence data were analyzed by using the GENETYX-MAC program (Software Development).

Structure Analysis

Crystals of ADH IIB were obtained by the sitting drop vapor diffusion method as described previously [43]. The protein (7.5 mg ml^{-1}) was mixed with an equal volume of the reservoir solution (14%–22% PEG8000, 150 mM sodium citrate, 100 mM HEPES-NaOH [pH 7.5], and 6% 2-propanol); crystallization was initiated by microseeding. The crystals are triclinic with cell parameters a = 54.8 Å, b = 57.4 Å, c = 67.5 Å, $\alpha = 89.6^\circ$, $\beta = 69.4^\circ$, $\gamma = 68.4^\circ$ and contain one molecule in the unit cell. X-ray data were collected from a native crystal at 100 K to 1.9 Å resolution. The data were 87% complete overall with R_{merge} = 6.4% and $I/\sigma(I) = 18.2$ (47.3% complete, $I/\sigma(I) = 4.2$ in the outer shell) as summarized in Table 4 (see [43]).

The native X-ray data were first analyzed by molecular replacement (MR) with AMORE [44] using MDH from *Methylophilus methylotrophus* W3A1 [12, 30] as the search molecule. A single peak in the rotation function established the orientation of the search model in the unit cell. An anomalous difference electron density map based on the MR phases contained two prominent peaks. One peak (14σ) was ~20 Å from the PQQ position in the MDH search molecule and was attributed to iron; the other (9σ) was attributed to calcium, being close to the position of the calcium ion in MDH that bridges PQQ and the protein side chains.

Two compounds, $K_3UO_2F_5$ and CH_3HgCl, showed 12%–15% isomorphous structure factor changes. MIR data from both derivatives were collected on image plates in the home laboratory while MAD data from the two derivatives were collected at the APS and SSRL synchrotrons, respectively (Table 4). Protein phases were calculated with SHARP [45] and improved by solvent flattening using the same program. Since the MIR maps were not sufficiently accurate, maps based on MIR and MAD phases combined in two ways (Table 4) were used. Before the ADH IIB sequence was known, the sequence of the *C. testosteroni* ADH quinoprotein domain [6] was fit to the electron density wherever possible, and polyalanine was fit elsewhere. The structure was partially refined using CNS [46] (40–3 Å resolution, R_{work} = 31%, R_{free} = 39% [47]).

When the PCR-derived sequence of ADH IIB was completed, it was fitted to the electron density map based on the combinations of MIR and MAD phases with the TURBO-FRODO program [48]. The model was refined using CNS first at 3 Å resolution and then extended to 2.5 Å and then to 1.9 Å resolution. A few rounds of minimization, including bulk solvent correction, B factor refinement, and model rebuilding, gave R_{work} = 0.236 and R_{free} = 0.261 at 1.9 Å resolution. Thereafter, water molecules were added interactively at the end of each refinement cycle to peaks over 3σ in height in the Fo-Fc electron density maps. After several iterations of minimization, B factor refinement, bulk-solvent correction, and model refitting, the final R_{work} and R_{free} were 0.154 and 0.189, with rmsd from ideal values of 0.006 Å for bond lengths and 1.43° for bond angles, respectively. The final model includes residues 1–664, one molecule each of PQQ, heme c, acetone, glycerol, HEPES, one calcium ion, and 732 water molecules. Four additional residues at the C terminus (Figure 2) were disordered and not included in the final model. The refinement statistics are summarized in Table 4. The result of PROCHECK [49] indicate that 86.1% of the residues are located in the most favorable regions, 13.0% in additional allowed regions, 0.5% in generously allowed regions, and 0.4% in disallowed regions.

Solvent-accessible surface areas were calculated by the method of Lee and Richards [50] as implemented in the program GRASP [41]. Protein alignments and rmsd calculations were carried out using the program LSQMAN [51]. Cavity volumes were computed with the program VOIDOO [52].

Acknowledgments

This work was supported by USPHS grants GM20530 and GM31611. This work was also supported by a Grant-in-Aid for Scientific Research (09044228) from the Ministry of Education, Science, Sports and Culture of Japan to K.M. We thank Ms. N. Aoki and Ms. Petra Baruch for their technical assistance and Professor Angelo Merli for making single-crystal microspectrophotometric measusrements. Use of the Argonne National Laboratory Structural Biology Center beamlines at the Advanced Photon Source was supported by the U.S. Department of Energy, Basic Energy Sciences, Office of Energy Research, under contract No. W-31-109-Eng-38. The portions of this research done at SSRL were supported by the U.S. Department of Energy, Office of Basic Energy Sciences and Office of Biological and Environmental Research, and by the NIH, National Center for Research Resources, Biomedical Technology Program, and the National Institute of General Medical Sciences.

Received: November 2, 2001
Revised: March 5, 2002
Accepted: March 11, 2002

References

1. Matsushita, K., and Adachi, O. (1993), Bacterial quinoproteins glucose dehydrogenase and alcohol dehydrogenase, In Principles and Applications of Quinoproteins, V.L. Davidson, ed. (New York: Marcel Decker) pp. 47–63.
2. Anthony, C. (1993), Methanol dehydrogenase in Gram-Negative bacteria, in Principles and Applications of Quinoproteins, V.L. Davidson, ed. (New York: Marcel Decker) pp. 17–45.
3. Matsushita, K., Toyama, H., and Adachi, O. (1994). Respiratory chains and bioenergetics of acetic acid bacteria. Adv. Microb. Physiol. *636*, 247–301.
4. Diehl, A., von Wintzingerode, F., and Gorisch, H. (1998). Quinoprotein ethanol dehydrogenase of *Pseudomonas aeruginosa* is a homodimer: sequence of the gene and deduced structural properties of the enzyme. Eur. J. Biochem. *257*, 409–419.
5. Toyama, H., Fujii, A., Matsushita, K., Shinagawa, E., Ameyama, M., and Adachi, O. (1995). Three distinct quinoprotein alcohol dehydrogenases are expressed when *Pseudomonas putida* is grown on different alcohols. J. Bacteriol. *177*, 2442–2450.
6. Groen, B., van Kleef, M.A.G., and Duine, J.A. (1986). Quinohemoprotein alcohol dehydrogenase apoenzyme from *Pseudomonas testosteroni*. Biochem. J. *234*, 611–615.
7. Yasuda, M., Cherepanov, A., and Duine, J.A. (1996). Polyethylene glycol dehydrogenase activity of *Rhodopseudomonas acidophila* derives from a type I quinohaemoprotein alcohol dehydrogenase. FEMS Microbiol. Lett. *138*, 23–28.
8. Shimao, M., Ninomiya, K., Kuno, O., Kato, N., and Sakazawa, C. (1986). Existence of a novel enzyme, pyrroloquinoline quinone-dependent polyvinyl alcohol dehydrogenase, in a bacterial symbiont, *Pseudomonas sp*. strain VM15C. Appl. Environ. Microbiol. *51*, 268–275.
9. Zarnt, G., Schrader, T., and Andreesen, J.R. (2001). Catalytic and molecular properties of the quinohemoprotein tetrahydrofurfuryl alcohol dehydrogenase from *Ralstonia eutropha* strain Bo. J. Bacteriol. *183*, 1954–1960.
10. Keitel, T., Diehl, A., Knaute, T., Stezowski, J.J., Hohne, W., and Gorisch, H. (2000). X-ray structure of the quinoprotein ethanol dehydrogenase from *Pseudomonas aeruginosa*: basis of substrate specificity. J. Mol. Biol. *297*, 961–974.
11. Matsushita, K., Yamashita, T., Aoki, N., Toyama, H., and Adachi, O. (1999). Electron transfer from quinohemoprotein alcohol dehydrogenase to blue copper protein azurin in the alcohol oxidase respiratory chain of *Pseudomonas Putida* HK5. Biochemistry *38*, 6111–6118.
12. Xia, Z.-X., Dai, W.-W., Zhang, Y.-F., White, S.A., Boyd, G.D., and Mathews, F.S. (1996). Determination of the gene sequence and the three-dimensional structure at 2.4 Å resolution of methanol dehydrogenase from *Methylophilus* W3A1. J. Mol. Biol. *259*, 480–501.
13. Ghosh, M., Anthony, C., Harlos, K., Goodwin, M.G., and Blake, C. (1995). The refined structure of the quinoprotein methanol dehydrogenase from *Methylobacterium extorquens* at 1.94 Å. Structure *3*, 177–187.
14. Oubrie, A., Rozeboom, H.J., Kalk, K.H., Olsthoorn, A.J., Duine, J.A., and Dijkstra, B.W. (1999). Structure and mechanism of soluble quinoprotein glucose dehydrogenase. EMBO J. *18*, 5187–5194.
15. Murzin, A.G. (1992). Structural principles for the propeller assembly of beta-sheets: the preference for seven-fold symmetry. Proteins *14*, 191–201.
16. Oubrie, A., and Dijkstra, B.W. (2000). Structural requirements of pyrroloquinoline quinone dependent enzymatic reactions. Protein Sci. *9*, 1265–1273.
17. Oubrie, A., Rozeboom, H.J., Kalk, K.H., Huizinga, E.G., and Dijkstra, B.W. (2002). Crystal structure of quinohemoprotein alcohol dehydrogenase from *Comamonas testosteroni*: structural basis for substrate oxidation. J. Biol. Chem. *277*, 3727–3732.
18. Datta, S., Mori, Y., Takagi, K., Kawaguchi, K., Chen, Z.W., Okajima, T., Kuroda, S., Ikeda, T., Kano, K., Tanizawa, K, et al. (2001). Structure of a quinohemoprotein amine dehydrogenase with an uncommon redox cofactor and highly unusual crosslinking. Proc. Natl. Acad. Sci. USA *98*, 14268–14273.
19. Satoh, A., Kim, J.K., Miyahara, I., Devreese, B., Vandenberghe, I., Hacisalihoglu, A., Okajima, T., Kuroda, S., Adachi, O., Duine, J.A. et al. (2002). Crystal structure of quinohemoprotein amine dehydrogenase from *Pseudomonas putida*. Identification of a novel quinone cofactor encaged by multiple thioether crossbridges. J. Biol. Chem. *277*, 2830–2834.
20. Altschul, S.F., Madden, T.L., Schaffer, A.A., Zhang, J., Zhang, Z., Miller, W., and Lipman, D.J. (1997). Gapped BLAST and PSI-BLAST: a new generation of protein database search programs. Nucleic Acids Res. *25*, 3389–3402.
21. Mathews, F.S. (1985). The structure, function and evolution of cytochromes. Prog. Biophys. Mol. Biol. *45*, 1–56.
22. Holm, L., and Sander, C. (1993). Protein structure comparison by alignment of distance matrices. J. Mol. Biol. *233*, 123–138.
23. Cunane, L.M., Chen, Z.-W., Shamala, N., Mathews, F.S., Cronin, C.N., and McIntire, W.S. (2000). Structure of the flavocytochrome *p*-cresol methylhydroxylase and its enzyme-substrate: gated substrate entry and proton relays support the proposed catalytic mechanism. J. Mol. Biol. *295*, 357–374.
24. Chen, L., Durley, R., Mathews, F.S., and Davidson, V.L. (1994). Structure of an electron transfer complex: methylamine dehydrogenase, amicyanin cytochrome c551i. Science *264*, 86–90.
25. Frazao C., Soares, C.M., Carrondo, M.A., Pohl, E., Dauter, Z., Wilson, K.S., Hervas, M., Navarro, J.A., De la Rosa, M.A., and Sheldrick, G.M. (1995). *Ab initio* determination of the crystal structure of cytochrome *c*6 and comparison with plastocyanin. Structure *3*, 1159–1169.
26. Than, M.E., Hof, P., Huber, R., Bourenkov, G.P., Bartunik, H.D., Buse, G., and Soulimane, T. (1997). *Thermus thermophilus* cytochrome-*c*552: a new highly thermostable cytochrome-c structure obtained by MAD phasing. J. Mol. Biol. *271*, 629–644.
27. Causer, M.J., Hopper, D.J., McIntire, W.S., and Singer, T.P. (1984). Azurin from *Pseudomonas putida*: an electron acceptor from p-cresol methylhydroxylase. Biochem. Soc. Trans. *12*, 1131–1132.
28. Chen, Z.W., Koh, M., Van Driessche, G., Van Beeumen, J.J., Bartsch, R.G., Meyer, T.E., Cusanovich, M.A., and Mathews, F.S. (1994).The structure of flavocytochrome *c* sulfide dehydrogenase from a purple phototrophic bacterium. Science *266*, 430–432.
29. Louie, G.V., and Brayer, G.D. (1990). High-resolution refinement of yeast iso-1-cytochrome *c* and comparisons with other eukaryotic cytochromes *c*. J. Mol. Biol. *214*, 527–555.
30. Zheng, Y.J. Xia, Z.-X., Chen, Z.-W., Mathews, F.S., and Bruice, T.C. (2001). Catalytic mechanism of quinoprotein methanol dehydrogenase: a theoretical and x-ray crystallographic investigation. Proc. Natl. Acad. Sci. USA *98*, 432–434.
31. Sato, A., Takagi, K., Kano, K., Kato, N., Duine, J.A., and Ikeda, T. (2001). Ca(2+) stabilizes the semiquinone radical of pyrroloquinoline quinone. Biochem. J. *357*, 893–898.
32. Zheng, Y.J., and Bruice, T.C. (1997). Conformation of coenzyme pyrroloquinoline quinone and role of Ca2+ in the catalytic mechanism of quinoprotein methanol dehydrogenase. Proc. Natl. Acad. Sci. USA *94*, 11881–11886.
33. Dewanti, A.R., and Duine, J.A. (2000). Ca2+-assisted, direct hydride transfer, and rate-determining tautomerization of C5-reduced PQQ to PQQH2, in the oxidation of beta-D-glucose by soluble, quinoprotein glucose dehydrogenase. Biochemistry *39*, 9384–9392.
34. Olsthoorn, A.J., and Duine, J.A. (1998). On the mechanism and specificity of soluble, quinoprotein glucose dehydrogenase in the oxidation of aldose sugars. Biochemistry *37*, 13854–13861.
35. Anthony, C. (1996). Quinoprotein-catalysed reactions. Biochem. J. *320*, 697–711.
36. Jongejan, A., Jongejan, J.A., and Hagen, W.R. (2001). Direct hydride transfer in the reaction mechanism of quinoprotein alcohol dehydrogenase: a quantum mechanical investigation. J. Comput. Chem. *22*, 1732–1749.
37. Beratan, D.N., Betts, J.N., and Onuchic, J.N. (1991). Protein electron transfer rates set by the bridging secondary and tertiary structure. Science *252*, 1285–1288.
38. Regan, J.J., Risser, S.M., Beratan, D.N., and Onuchic, J.N. (1993) Protein electron transport: single versus multiple pathways. J. Phys. Chem. *97*, 13083–13088
39. Blake, C.C., Ghosh, M., Harlos, K., Avezoux, A., and Anthony,

C. (1994). The active site of methanol dehydrogenase contains a disulphide bridge between adjacent cysteine residues. Nat. Struct. Biol. *1*, 102–105.

40. Avezoux, A., Goodwin, M.G., and Anthony, C. (1995). The role of the novel disulphide ring in the active site of the quinoprotein methanol dehydrogenase from *Methylobacterium extorquens*. Biochem. J. *307*, 735–741.
41. Nicholls, A., Sharp, K.A., and Honig, B. (1991). Protein folding and association: insights from the interfacial and thermodynamic properties of hydrocarbons. Proteins *11*, 281–296.
42. Zhang, Z., Huang, L., Shulmeister, V.M., Chi, Y.I., Kim, K.K., Hung, L.W., Crofts, A.R., Berry, E.A., and Kim, S.H. (1998). Electron transfer by domain movement in cytochrome bc_1. Nature *392*, 677–684.
43. Chen, Z.-W., Baruch, P., Mathews, F.S., Matsushita, K., Yamashita, T., Toyama, H., and Adachi, O. (1999). Crystallization and preliminary diffraction studies of two quinoprotein alcohol dehydrogenases (ADH): a soluble monomeric ADH from *Pseudomonas putida* HK5 (ADH IIB) and a heterotrimeric membrane-bound ADH from *Gluconobacter suboxydans* (ADH GS). Acta Crystallogr. D *55*, 1933–1936.
44. Navaza, J. (1994). AMoRe: an automated package for molecular replacement. Acta Crystallogr. *A50*, 157–163.
45. de La Fortelle, E., and Bricogne, G. (1997). Maximum-likelihood heavy-atom parameter refinement in the MIR and MAD methods. Methods Enzymol. *276*, 472–494.
46. Brunger, A.T., Adams, P.D., Clore, G.M., DeLano, W.L., Gros, P., Grosse-Kunstleve, R.W., Jiang, J.S., Kuszewski, J., Nilges, M., Pannu, N.S., et al. (1998). Crystallography & NMR system: a new software suite for macromolecular structure determination. Acta Crystallogr. D Biol. Crystallogr. *54*, 905–921.
47. Kleywegt, G.J., and Brunger, A.T. (1996). Checking your imagination: applications of the free R value. Structure *4*, 897–904.
48. Roussel, A., Fontecilla-Camps, J.C., and Cambillau, C. (1990) CRYStallize: a crystallographic symmetry display and handling subpackage in TOM/FRODO. J. Mol. Graph. *8*, 86–88.
49. Morris, A.L., MacArthur, M.W., Hutchinson, E.G., and Thornton, J.M. (1992). Stereochemical quality of protein structure coordinates. Proteins *12*, 345–364.
50. Lee, B., and Richards, F.M. (1971). The interpretation of protein structures: estimation of static accessibility. J. Mol. Biol. *55*, 379–400.
51. Kleywegt, G.J., and Jones, T.A. (1997). Detecting folding motifs and similarities in protein structures. Methods Enzymol. *277*, 525–545.
52. Kleywegt, G.J., and Jones, T.A. (1994). Detection, delineation, measurement and display of cavities in macromolecular structures. Acta Crystallogr. D *50*, 178–185.
53. Kraulis, P.J. (1991). MOLSCRIPT: a program to produce both detailed and schematic plots of protein structures. J. Appl. Crystallogr. *24*, 946–950.
54. Merritt, E.A., and Bacon, D.J. (1997). Raster3D: photorealistic molecular graphics. Methods Enzymol. *277*, 505–524.

Accession Numbers

Coordinates of ADH IIB from *Psuedomonas putida* HK5 have been deposited in the Protein Data Bank with accession code 1KV9.